

Structure, Mechanical, and Tribological Properties of MoS₂/a-C:H Composite Films

Yanxia Wu · Hongxuan Li · Li Ji · Liu Liu ·
Yinping Ye · Jianmin Chen · Huidi Zhou

Received: 12 November 2012 / Accepted: 3 September 2013 / Published online: 13 October 2013
© Springer Science+Business Media New York 2013

Abstract A series of hydrogenated amorphous carbon (a-C:H) films doped with molybdenum disulfide (MoS₂) were deposited by medium frequency unbalanced magnetron sputtering with mixed Ar/CH₄ gases of different volume ratios as the source gases. The effects of Ar/CH₄ ratio on morphology, microstructure, mechanical, and tribological properties of the MoS₂/a-C:H composite films were investigated. Results show that the content of MoS₂ in the as-deposited films decreases with the decreasing Ar/CH₄ ratio, and the highest Ar/CH₄ ratio favors the formation of nanostructured films. Besides, the hardness and internal stress of the composite films first decrease and then increase with decreasing Ar/CH₄ ratio. Furthermore, the film deposited at the highest Ar/CH₄ ratio exhibits excellent antiwear ability in all test environments and shows promising potential as a solid lubricating film in aviation and space industries.

Keywords MoS₂/a-C:H film · Ar/CH₄ ratio · Tribological properties

Y. Wu · H. Li (✉) · L. Ji · Y. Ye · J. Chen (✉) · H. Zhou
State Key Laboratory of Solid Lubrication, Lanzhou Institute of
Chemical Physics, Chinese Academy of Sciences,
Lanzhou 730000, China
e-mail: lihx@licp.cas.cn

J. Chen
e-mail: chenjm@ns.lzb.ac.cn; chenjm@licp.cas.cn

Y. Wu
Graduate University of Chinese Academy of Sciences,
Beijing 100049, China

L. Liu
College of Life-Science and Chemistry, Tianshui Normal
University, Tianshui 741001, China

1 Introduction

Space-born systems cover a broad range of contact stresses from 10⁷ to 10¹⁰ Pa and sliding speeds from near zero in restraining mechanisms to above 20 m/s in control-moment gyros. Space applications can be exposed to moisture during assembly, ground tests, or launch, and contact atomic oxygen in low earth orbit or vacuum in high earth orbit where all demand a long service life in various test environments [1]. Therefore, the mechanical, environmental, and endurance requirements of space applications exceed the available lubrication and wear reduction technologies, demanding novel materials and advanced technologies. Low outgassing liquids are used when tribo-assembly can be sealed from the outside environment, and the preferred solid lubricants are the predominant materials used for space lubrication [2]. Due to the high hardness, low friction, and low wear, amorphous hydrogenated carbon (a-C:H) film is often referenced as a potential space tribological material [3, 4]. However, the short sliding lifetime of a-C:H film in heavily loaded, and/or high sliding speed applications in vacuum be a must issue for its application [5]. Although some researches were performed on the a-C-based lubrication to prolong the sliding lifetime of the film in vacuum [1, 6–8], fewer reports are about a-C:H film [9, 10]. As reported before [9], the composite films consisted of a-C:H and molybdenum disulfide (MoS₂) can prevent the oxidation of the MoS₂ during the storage period and prolong the sliding lifetime of a-C:H film in vacuum. However, the relationship between the structure, mechanical, and tribological properties of the film is not investigated in detail.

In this study, we have successfully fabricated MoS₂/a-C:H composite films with mixed Ar/CH₄ gases of different volume ratios as the source gases by medium frequency

unbalanced magnetron sputtering technique. The surface morphology, microstructure, mechanical, and tribological properties of the films were investigated by various analytical techniques. The results revealed that the film deposited at the highest Ar/CH₄ ratio (sccm/sccm) shows highest content and stoichiometric ratio of S and Mo, as well as the hardness and excellent wear-resistance performances in various environments.

2 Experimental Details

2.1 Deposition of MoS₂/a-C:H Composite Films

A series of MoS₂/a-C:H composite films were deposited by unbalanced magnetron sputtering (SP-0806SI) technique with Ar (purity 99.9 %) and CH₄ (purity 99.9 %) as sputtering gases of two graphite targets (size 94 × 300 mm², purity 99.9 %) and one molybdenum disulfide target (purity 99.9 %). The composite films deposited on the stainless steel were used for friction and wear tests, and those deposited on Si p(111) substrate were used for characterization. Prior to film deposition, the substrates were cleaned ultrasonically in an acetone bath and dried in air. Then, they were assembled in the substrate holder which is 20 cm away from the sputtering targets, followed by plasma etching with Ar⁺ ions in a vacuum chamber to remove the native oxide on the substrates' surface. Details of the deposition system were reported before [11]. The substrate holder kept revolving (5 rev/min) during the deposition process, which would be beneficial to improve the uniformity of the composite films. The chamber temperature during the deposition was about 65°C for the deposition of the film. A Si target (99.99 %) was connected to DC power supply to deposit a Si interlayer. Prior to the film deposition, the silicon interlayer, about 200 nm thick, was deposited on substrates by magnetron sputtering (a target current of 8 A) to improve the adhesion between the substrate and film. Then, the film deposition was performed under substrate bias voltage of −200 V with duty cycle of 20 %, MoS₂ target current of 0.6 A, and graphite target current of 14 A. The typical gas pressure during the film deposition was about 0.53 Pa with Ar/CH₄ gases of different volume ratios (105/5, 95/15, 80/30, and 65/45). The deposition time was 2 h and the thickness of the film was in the range of 1.5–1.8 μm. Special sample for TEM analysis was grown directly on the freshly cleaved single-crystal NaCl wafers.

2.2 Characterization of MoS₂/a-C:H Composite Films

The composition of the film was determined using a multifunctional X-ray photoelectron spectroscope (XPS,

operating with Al-Kα radiation and detecting chamber pressure of below 10^{−8} torr). The film was etched 3 min by Ar⁺ ion to ensure that the tested material represented bulk coating. The atom concentration of the samples was calculated from XPS signals corresponding to Mo(3d), S(2s), Au(1s), and C(1s) core levels using the standard sensitivity factors of the instrument. The bonding structure information of the MoS₂/a-C:H film was obtained by Jobin–Yvon HR-800 Raman spectrometer at an argon-ion laser source power density of 0.1 mW/m², having wavelength of 532 nm. Fourier transformation infrared (FTIR) spectra of the composite film were recorded on a FTS165 spectrometer to detect the changes in the bonded hydrogen content.

A digital instrument Nanoscope IIIa multimode atomic force microscope (AFM) in tapping mode was performed to observe the surface morphology of the films. The average surface roughness over an area of 3.0 μm × 3.0 μm was calculated using the software attached to AFM. A JEOL 2010 transmission electron microscope (TEM) was performed at an accelerating voltage of 200 kV to record high-resolution TEM images (HRTEM) of MoS₂/a-C:H film samples that were first deposited on NaCl substrate and then collected for TEM analysis after NaCl substrate was dissolved in distilled water.

The hardness value of the composite film was determined using a NanoTest 600 nanomechanical system (MicroMaterials Ltd, UK), where the maximum indentation depth was controlled to be about 150 nm (<10 % of film thickness) so as to minimize the effect of the substrate. The curvature radius of the composite film was measured using a MicroXAM surface mapping microscope (ADE shift, America), and the internal stress was calculated based on the Stoney equation [12]:

$$\sigma = \frac{E_s}{6(1 - \nu_s)} \left(\frac{t_s^2}{t_f} \right) \left(\frac{1}{R_2} - \frac{1}{R_1} \right)$$

where σ is the internal stress, R_1 and R_2 are the substrate curvature radii before and after film deposition, ν_s and E_s are Poisson's ratio and Young's modulus of the substrate, and t_s and t_f are the thickness of the substrate and film [13], respectively. A Micro XAM 3D non-contact surface profilometer was used to measure the thickness. Microscratch tests were carried out using a MFT-4000 friction-monitored scratch tester equipped with acoustic emission (AE) resonance sensors. During the test, a linearly increasing load was applied to a static indenter at a loading rate of 25 N/min. At the same time, the friction force was recorded and displayed as a function of load. The first derivation of the friction force was also calculated to provide a clear indication of the change in friction force. The critical load was defined as the load at which the friction force suddenly increased and surface layer failure occurred. A Rockwell indenter with a radius of 0.1 mm was used in the test, and

the scratch load started from 0 N and stopped immediately after reaching the critical load.

2.3 Ball-on-Disk Friction and Wear Test

The tribological property tests the as-deposited composite films that were evaluated with a ball-on-disk tribometer. The photograph and schematic diagram of the apparatus have been described elsewhere [14]. The steel balls (GCr15, Φ 6 mm) were used as the counterpart. Briefly, sliding tests of the films against counterpart ball were run at a normal load of 5 N, a sliding speed of 5 rev/s, and a wear track radius of 6 mm at a room temperature about 20 °C. When tested in vacuum, a vacuum degree of 5.0×10^{-3} Pa was attained in the chamber with a turbomolecular pumping system. Before each friction and wear test, the frictional pair was ultrasonically cleaned with acetone. All the tests were commenced to a maximum sliding duration of 3,600 s. Friction experiments were conducted thrice under each experimental condition. The worn surface of the film was characterized by Micro XAM 3D non-contact surface profilometer. The corresponding counterparts were characterized by JSM-5600LV scanning electron microscope (SEM) or the Olympus STMT measuring microscope.

3 Results and Discussion

3.1 Composition and Bonding Structure

The deposition conditions and chemical compositions of as-deposited MoS₂/a-C:H films are shown in Table 1. The chemical composition was calculated without oxygen because it was difficult to measure due to a progressive surface oxidation of the samples. It can be seen that the contents of Mo and S mainly decrease with the decreasing ratio of Ar/CH₄, whereas the carbon content in the film increases. The effect of Ar/CH₄ ratio on the composition of the film can be regarded as the carbon in the composite film comes from two sources, the particles sputtered from graphite target and the radicals decomposed by CH₄

molecules. Generally, the CH₄ molecules are decomposed into some hydrocarbon neutral radicals (CH, CH₂, CH₃), ionic radicals (CH⁺, CH₃⁺, C₂H₅⁺), and atomic or ionic hydrogen during the deposition [15]. Under high Ar/CH₄ ratio, the increased Ar⁺ bombarding the targets and the decreased target poison increase the ionization degree of the CH₄ molecules, increasing the fraction of high energetic H⁺ in the plasma and combining with the S²⁻ to form H₂S. Meanwhile, the high sputtering yield of graphite and MoS₂ make more particles in the formation of the composite films. With decreased Ar/CH₄ ratio, as a result of increased CH₄ content, on the one hand, the radicals with low ionization degree and high atomic mass (C_xH_y) decomposed by CH₄ trapped on the growing surface increase and thus increase in the carbon content; on the other hand, the target poison is so serious that the ion sputtering yields of the graphite and MoS₂ are very low, and the resulted decreasing sputtering yield of targets makes less graphite, Mo, and S particles participate in the formation of composite films. The S/Mo ratio varied in the range of 0.91–1.95 and mainly decreases with the decreasing Ar/CH₄ ratio. Sub-stoichiometry of S and Mo in the deposited film is typically attributed to both the reaction of the sulfur with the residual atmosphere (particularly H₂ and O₂) and the preferential resputtering effect of sulfur due to the bombardment of neutral argon atoms reflected in the target during the sputtering process [16]. Additionally, the ionic hydrogen decomposed by CH₄ may combine with the S²⁻ sputtered by MoS₂ to form H₂S during the deposition, thus relatively low stoichiometric proportion of S and Mo in the composite film. Figure 1 shows the C1s, S2p, and Mo3d XPS spectra of the composite films deposited at different Ar/CH₄ ratios. The peak in C1s spectra around 284.6 eV corresponds to C–C bond. The peak observed at 161.6 eV in S2p spectra indicates the sulfur in the MoS₂. The Mo3d spectra consist of peaks at around 227.7 and 230.8 eV corresponding to Mo⁴⁺ 3d_{3/2} and Mo⁴⁺ 3d_{5/2}, respectively [17]. It can be seen that the MoS₂ contribution is still dominant in the Mo3d spectrum, which indicates that there was no oxidation in the film bulk. There was no MoC peak found in the C1s and Mo3d spectra, which indicates no MoC formed in the composite films [16].

Infrared spectroscopy is widely used to characterize C–H bonding of the a-C:H-based films, in which the intensity of C–H absorption peak is an indication of the content of bonded hydrogen. IR transmission spectra of the composite films deposited at different Ar/CH₄ ratios are plotted in Fig. 2. The spectra of the films deposited at lower Ar/CH₄ ratios include a main peak at 2,920 cm⁻¹ belonging to sp³ CH and sp³ CH₂ asymmetric stretching modes, and two smaller shoulder peaks at 2,950 and 2,870 cm⁻¹ corresponding to sp³ CH₃ asymmetric and symmetric stretching

Table 1 Deposition conditions and the chemical composition of the films deposited at different Ar/CH₄ ratios

Ar/CH ₄ ratio (sccm/sccm)	Chemical composition (at %)			[S]/[Mo]	
	C	Mo	S		
105	5	85	5.07	9.93	1.96
95	15	87.39	4.36	8.24	1.89
80	30	91.14	3.33	5.54	1.66
65	45	93.08	3.62	3.3	0.91

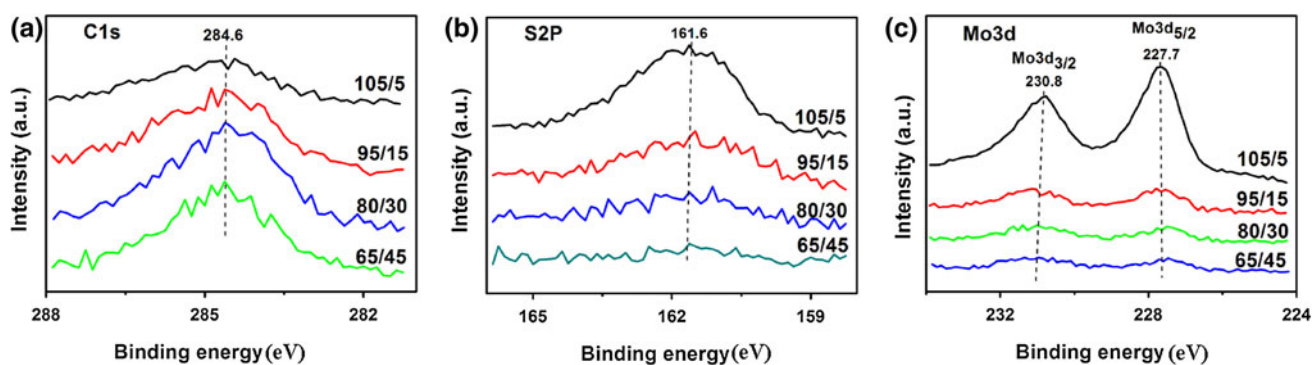


Fig. 1 XPS spectra of MoS₂/a-C:H composite films deposited at different Ar/CH₄ ratios: **a** C1s; **b** S2p; **c** Mo3d

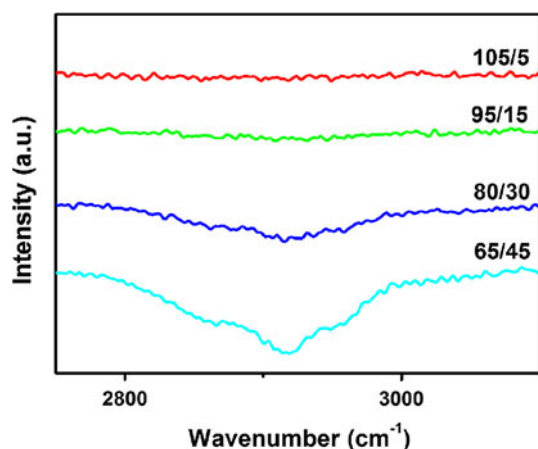


Fig. 2 IR transmission spectra of MoS₂/a-C:H composite films prepared at different Ar/CH₄ ratios

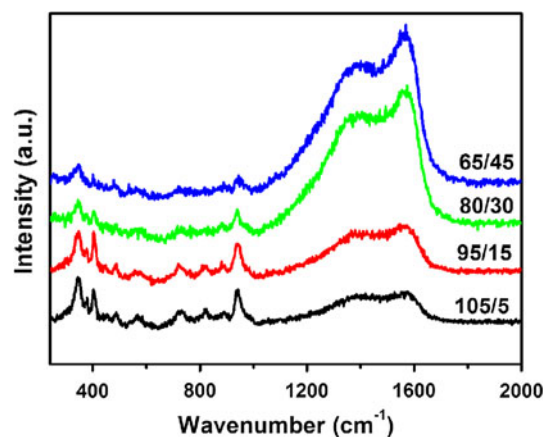


Fig. 3 Raman spectra of MoS₂/a-C:H composite films prepared at different Ar/CH₄ ratios

modes, respectively [18, 19]. For the films deposited at higher Ar/CH₄ ratios, there were no peaks in the spectra indicating that there was almost no bonded hydrogen in the film, which is due to the increased ionization degree of the CH₄ molecules when there was less CH₄ in the source gases. The increasing fraction of high energetic H⁺ decomposed by CH₄ in the plasma may combine with S²⁻ to form H₂S or exist in the form of free hydrogen, and thus, almost no hydrogen bonded with C in the film. At lower Ar/CH₄ ratios, the target was poisonous seriously and the sputter yields of the targets were lower. However, the radicals with low ionization degree and high atomic mass (C_xH_y) decomposed by CH₄ trapped on the growing surface increased and thus increase in the bonded hydrogen content.

Raman spectroscopy is a popular and effective tool for the characterization of carbon-based films. There were two evident pairs of peaks corresponding to carbon (approx. at 1,410 and 1,570 cm⁻¹) and MoS₂ (approx. at 370 and 410 cm⁻¹, see Fig. 3). The peak at ~820 cm⁻¹ is identified as MoO₃, which indicates the oxidation on the surface of composite film. It can be seen that the content of MoS₂ decreases, whereas carbon increases with the decreasing

Ar/CH₄ ratio, which is consistent with the XPS results. The Raman spectroscopy of carbon-based film can indirectly derive the sp³ fraction depending on the linkage of sp² and sp³ phases. There were two evident pairs of peaks corresponding to carbon (*G* peak around 1,350 cm⁻¹ and *D* peak around 1,550 cm⁻¹). The *G* peak of the film is due to the carbon bond stretching of all pairs of sp² atoms in both rings and chains, and the *D* peak is due to the breathing modes of sp² atoms in rings. Many previous studies [20–22] have shown that the sp³ fraction of the films can be calculated from the wave number and the intensity of the *G* and *D* peaks. As the sp³ fraction decreases, the *G* peak shifts toward higher wavelength and the ratio of *I*_(D)/*I*_(G) increases. Figure 4 shows the corresponding *I*_(D)/*I*_(G) ratio and the *G* peak position of the composite films. It can be seen that the *D* peak intensities are greatly decreased and the *G* peak shifts toward lower wavelength, indicating the lower fraction of sp²-bonded carbon in the composite films with decreasing Ar/CH₄ ratio. On the one hand, the Mo particles generated by sputtering MoS₂ target play a role of catalyst which can lead to the conversion of sp³ hybrid carbon into sp² hybrid carbon as reported before [11]; and

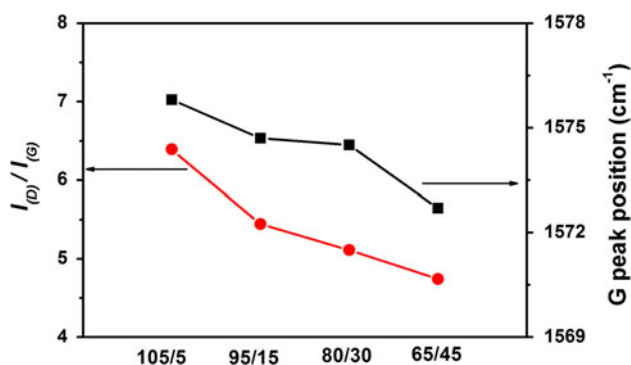


Fig. 4 Corresponding $I_{(D)}/I_{(G)}$ ratio and the G peak position of $\text{MoS}_2/\text{a-C:H}$ composite films prepared at different Ar/CH_4 ratios

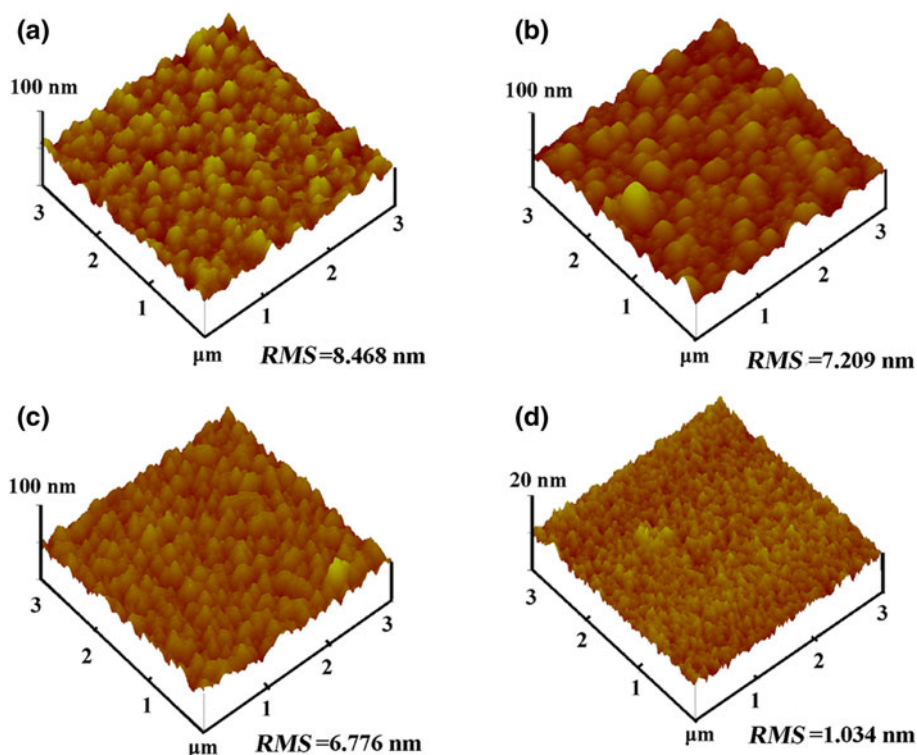
on the other hand, with higher MoS_2 content, the bombardment of relatively heavy ions would lead to dispersion of more energy on the growing film surface, similar to the case of heavy metal (copper, erbium, titanium, etc) doping, which is propitious to the formation of sp^2 hybrid carbon [11, 23, 24]. It also implies the change of sp^2 cluster from dimmers and chains to rings because the doping of MoS_2 in amorphous carbon matrix degrades the fraction of bridging sp^3 hybrid carbon concentration in the film [21]. For the film with high content of MoS_2 , most of the sp^2 clusters in the composite films are present in the form of chains or dimers, corresponding to a high volume of grain boundaries (polyacetylene-type structural units) around MoS_2 crystalline nanoparticles therein which will be confirmed

by HRTEM [25]. It is possible that the doping of MoS_2 in the film leads to the formation of more sp^2 clusters, and these clusters would be expected to be stacked, forming graphite-like structure with crystallinity on the nanoscale.

3.2 Surface Morphology

Figure 5 shows the three-dimensional AFM images of as-deposited $\text{MoS}_2/\text{a-C:H}$ composite films deposited at different Ar/CH_4 ratios. All the films have relatively high root mean square (RMS) roughness that originated from the MoS_2 particles except the one deposited at $\text{Ar}/\text{CH}_4 = 65/45$, and they contain small spheres, and the size of the spherical particles decrease with decreasing Ar/CH_4 ratio. First, the film deposited at high volume ratio of Ar/CH_4 contains more MoS_2 particles that are much bigger than carbon particles, thus a relatively high surface roughness; second, at lower CH_4 content, the increased Ar^+ bombarding the target and the decreased target poison increase the particle with higher ion energy that is in favor of the formation of islands with big size due to the surface tension effects; and third, the film deposited at higher Ar/CH_4 ratio contains more sp^2 cluster as shown in Raman spectra, and the formation of sp^2 cluster on the film surface can increase the surface roughness via subsurface atom diffusion during the deposition processes as reported [15, 26]. At the lowest Ar/CH_4 ratio, the film has lowest MoS_2 content and sp^2

Fig. 5 AFM images of as-deposited $\text{MoS}_2/\text{a-C:H}$ composite films prepared at different Ar/CH_4 ratios: **a** 105/5; **b** 95/15; **c** 80/30; **d** 65/45



cluster in the film as shown in XPS and Raman spectra. Meanwhile, the bombarding of ion is lowest and the bonded hydrogen is highest, so the film resembled “amorphous hydrogenated carbon-like film” and thus a relatively low roughness about 1.0 nm.

Figure 6 shows the HRTEM images of the composite films deposited at $\text{Ar}/\text{CH}_4 = 105/5$ and $65/45$, respectively. It can be seen that for the film deposited at highest Ar/CH_4 ratio, there were some nanoclusters inhomogeneously embedded in the amorphous carbon matrix, the nanoparticles had a size of about 10 nm, and a high volume of grain boundaries was well around the hexagon-shaped nanoparticles. The corresponding selected area electron diffraction (SAED) pattern of the composite films displayed three rings that are well indexed as MoS_2 {002}, {100}, and {006}, respectively, which confirms the formation of nanocrystalline MoS_2 in a-C cross-linked matrix. However, the crystallinity was poor. For the film deposited at the lowest Ar/CH_4 ratio, neither of the images shows crystalline nor diffraction rings, which confirms that the film was amorphous and resembles “amorphous hydrogenated carbon-like film.”

3.3 Mechanical Properties

The internal stress of as-deposited $\text{MoS}_2/\text{a-C:H}$ films deposited with mixed Ar/CH_4 gases of different volume ratios is shown in Fig. 7. It is seen that all the films had

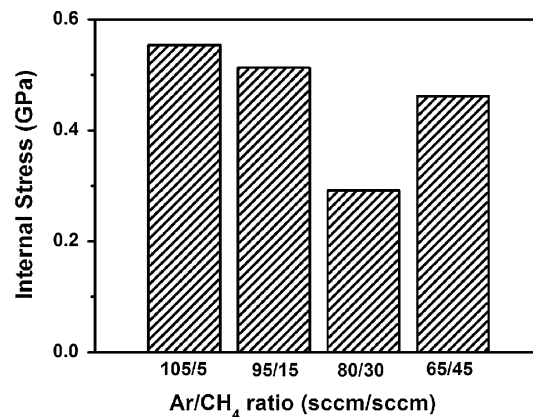


Fig. 7 Internal stress of as-deposited $\text{MoS}_2/\text{a-C:H}$ films deposited with mixed Ar/CH_4 gases of different volume ratios

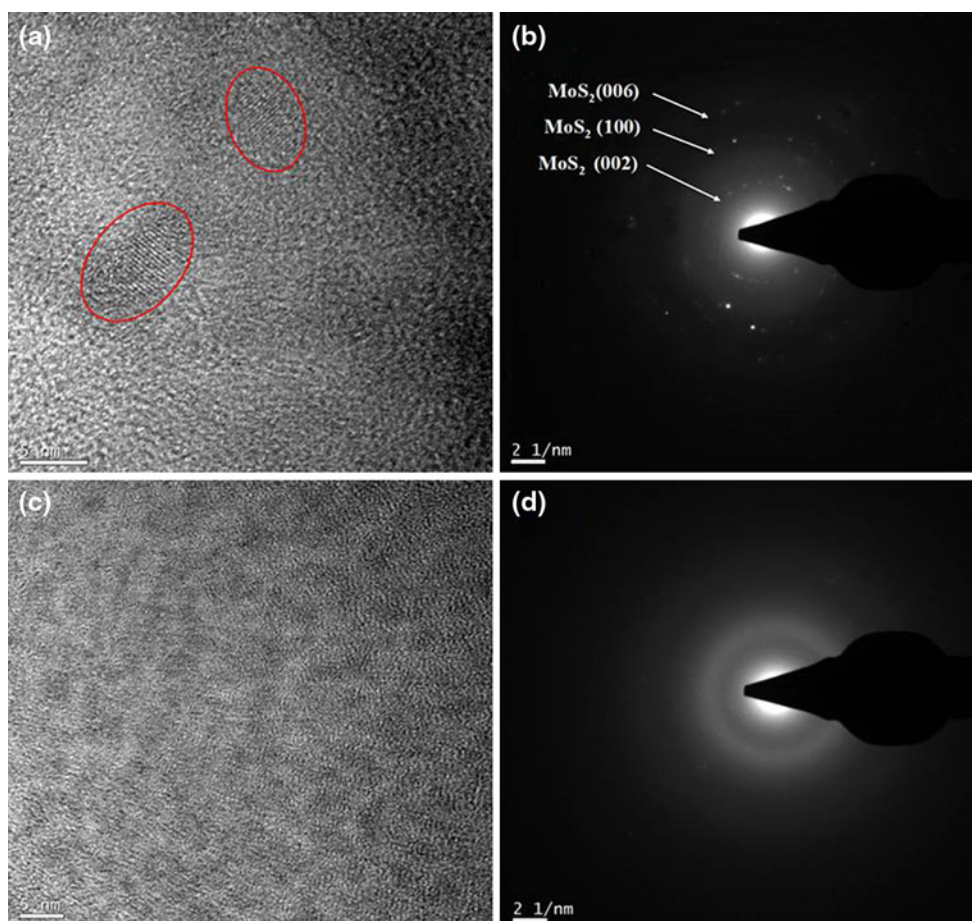


Fig. 6 HRTEM images and the corresponding SAED patterns of $\text{MoS}_2/\text{a-C:H}$ composite films deposited at different Ar/CH_4 ratios: **a, b** $\text{Ar}/\text{CH}_4 = 105/5$; **c, d** $\text{Ar}/\text{CH}_4 = 65/45$

relatively low compressive stresses. The internal stress of the composite film decreased first and then increased with the decreasing volume ratio of Ar/CH₄ gases. As is known, the compressive stress in the carbon-based films is mainly derived from the formation of sp³ sites [27]. The doping of MoS₂ may lead to a high sp² content (as evidenced by the Raman spectra) and thus relatively low internal stress for the composite films compared with the reported amorphous hydrogenated carbon film [28]. Moreover, the nanocrystalline in the film is beneficial to generate a high density of interfaces and a high volume of grain boundaries which can relax internal stress by diffusion and sliding. The first decreased internal stress with the decreasing Ar/CH₄ ratio can be explained as follows: On the one hand, with the decreasing Ar/CH₄ ratio, the decreased bombarding effect of Ar⁺ caused the great decrease in the compressive stress; and on the other hand, the increasing CH₄ ratio causes serious target poison and leads to the low ionization degree of hydrocarbon particles, and the radicals with high atomic mass (C_xH_y) and low energy are trapped on the surface and form the loose cross-linking structure, so the internal stress becomes low. Decreasing the Ar/CH₄ ratio further can cause serious target poison, the rarely sputtered S²⁻ particle was almost combined with the H⁺ in the radicals with high atomic mass (C_xH_y) to form H₂S, and some radicals may lead to the increase in atomic packing density and thus a relatively high compressive stress. It can be confirmed by the small content of Mo and S detected by XPS spectra. Moreover, the film resembles “amorphous hydrogenated carbon film” as shown in Raman and IR spectra and thus a relatively high internal stress.

The adhesion results of the film are given in Fig. 8, and the critical load is usually used to evaluate the adhesion strength between the film and substrate. It can be seen that with decreasing Ar/CH₄ ratio (decreasing MoS₂ content), the critical load of the films decreases. It is known that the improvement of the adhesion can be achieved by a high

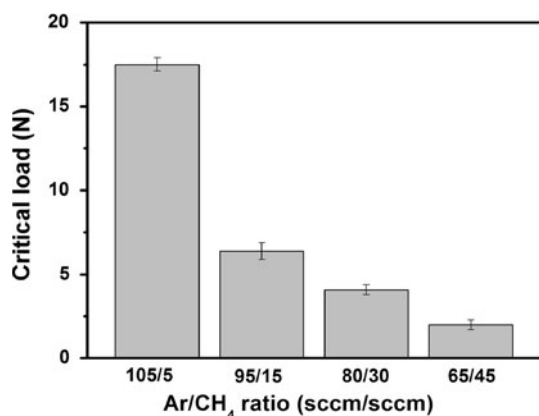


Fig. 8 Critical load of the MoS₂/a-C:H films deposited by different Ar/CH₄ ratios

density of covalent interface bonds, a low interface stress, and a low total internal stress [29]. Since the internal stress of the films does not show the same trend as the adhesion results, the adhesion result is mainly affected by the covalent interface bond. The films deposited at higher Ar/CH₄ ratios have more MoS₂ and sp² C contents, and less H and sp³ C contents (Figs. 2, 3). All these are inclined to form more bonds with the silicon interlayer and thus high adhesion strength. Furthermore, more MoS₂ particles in the films increase the effective area during the deposition, offering a higher number of possible adhesive bonds [29].

Figure 9 depicts the hardness and elastic modulus of MoS₂/a-C:H composite films deposited with mixed Ar/CH₄ gases of different volume ratios. The hardness of the composite films reduces from 5.1 to 2.3 GPa and then increases to 4.2 GPa with decreasing Ar/CH₄ ratio, and their elastic modulus also varies in the same manner. As reported before, when the nanocrystalline/amorphous system has 3–10 nm crystalline grains dispersed in an amorphous matrix and the grains are separated by 1–3 nm amorphous matrix, the nanocomposite structure can help to increase the strength of the films by preventing the operation of dislocation sources, restraining the existing dislocations in adjusted nanophases with different elastic constants, and building up material volume energy from grain boundary incoherent strains and thus a high hardness [30]. The decreasing tendency in hardness of composite films is due to the decreased harden effect because of the decreased MoS₂ nanoparticles in the film with decreasing Ar/CH₄ gases. For the film deposited at lowest Ar/CH₄ ratio, the film resembles “amorphous hydrogenated carbon-like film,” and the distortion of the bond lengths and angle in the sp² carbon rings decreases as demonstrated by Raman analysis, which is favorable for the connectivity of carbon atoms in various existing sites and hence increased hardness [31].

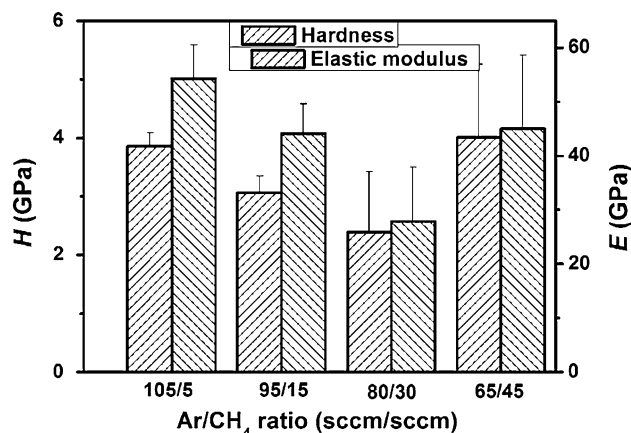
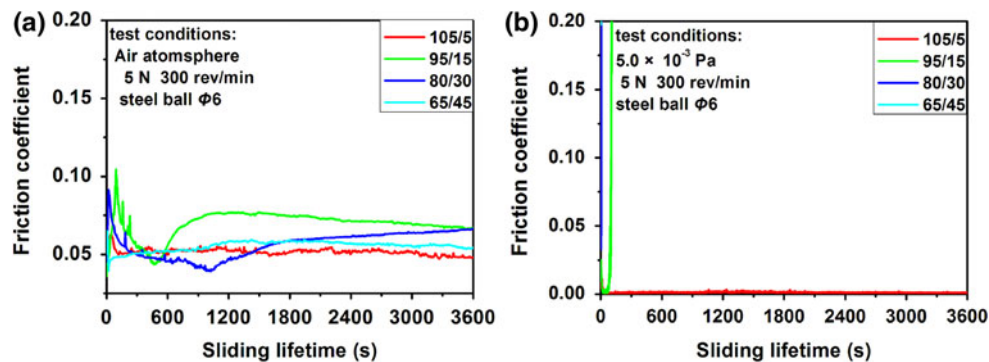


Fig. 9 Hardness and elastic modulus of MoS₂/a-C:H composite films deposited with mixed Ar/CH₄ gases of different volume ratios

Fig. 10 Tribological curves of MoS₂/a-C:H composite films tested in different environments: **a** air; **b** vacuum



3.4 Tribological Properties

The influence of Ar/CH₄ ratios on the tribological properties of MoS₂/a-C:H composite film was evaluated with a pin-on-disk tribometer. Figure 10 shows the tribological performances of the composite film sliding against steel balls in different test environments (air and vacuum). It can be seen that both the test environment and Ar/CH₄ volume ratio have significant effects on the tribological behavior of the composite film. When the films are tested in air, they show friction coefficients ranging from 0.05 to 0.08 and sliding lifetime longer than 3,600 s, and the film deposited at Ar/CH₄ = 105/5 shows the lowest friction coefficient. In vacuum environment, most of the films have extremely short sliding lifetime. However, the film deposited at Ar/CH₄ = 105/5 has extremely low friction coefficient of 0.002 and the longest sliding lifetime than 3,600 s. It can be seen that the film deposited at Ar/CH₄ = 105/5 exhibits the best tribological properties in all test environments.

The worn surface and the corresponding counterpart of the films tested in air are given in Fig. 11. As shown in Fig. 11, with decreasing MoS₂ content in the composite film (decreasing Ar/CH₄ ratio during the film deposition),

the wear track on the film becomes deeper and the wear scar on the counterpart becomes broader, correspondingly. The worn surface of the film deposited at Ar/CH₄ = 105/5 is mild, with some slight scratches. The corresponding contact area of the counterpart is covered by dense and much attenuated wear debris. In this case, the good tribological behavior is mainly attributed to the higher adhesion strength and the formation of the transferred materials on the counterpart ball, which may periodically form and lose during the friction test. The high friction coefficient and severe wear of the film deposited at Ar/CH₄ = 65/45 may originate from the serious plowing effect caused by the hard wear debris entrapped in the contact region of both the film and the mated ball (which is possible as there are no obvious transfer layers formed, and only a few transferred materials can be found at the center of the mated ball, as shown in Fig. 11h).

In order to gain more insight into the friction and wear mechanisms of the composite films in vacuum, the worn surface of the films (deposited at Ar/CH₄ = 105/5 and 65/45), as well as the counterpart balls, was studied by 3D surface profilometry and scanning electron microscope, respectively. As shown in Fig. 12, the worn surfaces of the

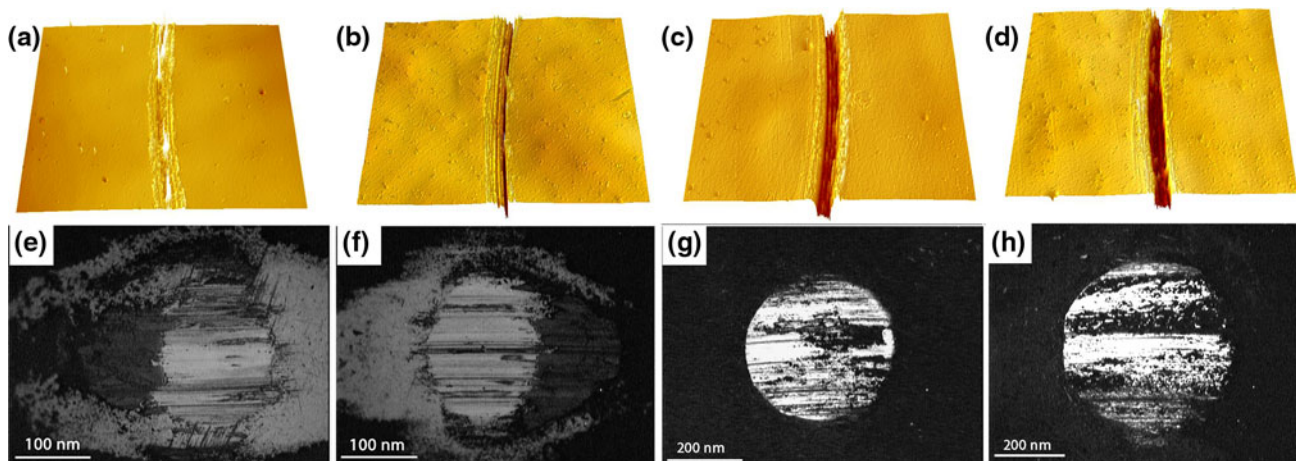


Fig. 11 Worn surfaces of the films deposited at different Ar/CH₄ ratios and the corresponding counterparts after tests in air: **a**, **e** 105/5, **b**, **f** 95/15, **c**, **g** 80/30, **d**, **h** 65/45

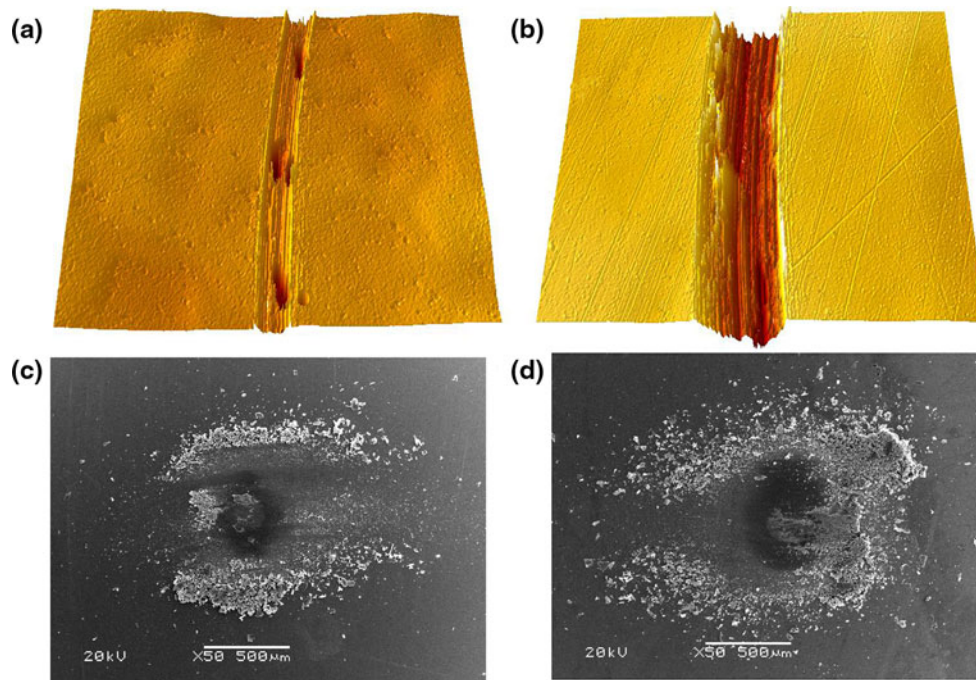


Fig. 12 Worn surfaces of the films deposited at different Ar/CH₄ ratios and the corresponding counterparts after tests in vacuum: **a, c** 105/5, **b, d** 65/45

films are characterized by furrows with different widths and depths. It can be clearly seen that the film deposited at Ar/CH₄ = 105/5 shows narrower and shallower furrow, compared with the film deposited at 65/45, which was worn out. Moreover, the worn surface of the film deposited at Ar/CH₄ = 105/5 is featured by local peeling except for the furrow. This may be due to the abrasive wear during the sliding because of the hard carbon phase, accompanied with the defect in the film. The wear scar on the counterpart ball sliding against the film deposited at Ar/CH₄ = 105/5 is relatively small and slight, with a compacted transfer film over it. However, the worn surface on the counterpart ball sliding against the film deposited at Ar/CH₄ = 65/45 has no uniform transfer film formed with large wear debris scattered around the wear scar. The formation of transfer film, especially for the stable one, would greatly affect the tribological properties of the testing material [5]. It could support loading and reduce wear more effectively. More importantly, the poor adhesion caused the film break away from substrate during the early stage of the friction testing, which is directly responsible for the shortest wear life.

Combined with the structural analysis, not only the [S]/[Mo] but also the concentration of sulfur and molybdenum should be optimized for super-low friction in vacuum. The composite film exhibits super-low friction in vacuum because the MoS₂ lamellar structures could be formed between ball and coating during friction [9]. Moreover, the nanocrystalline/amorphous system of packing MoS₂ by

amorphous carbon is a good candidate for preventing oxidation of the clusters; the MoS₂ transfer layer is formed by an amorphous-to-crystalline transformation of dichalcogenide inclusions whose rubbing orients the crystalline material such that the low friction basal plane is parallel to the surface. A graphitic-like transfer layer is formed by sp³ to sp² phase transition of a-C:H component in air environment, which eventually leads to the formation of some crystalline graphite and provides a low friction coefficient and significantly reduces further wear.

4 Conclusion

A series of MoS₂/a-C:H composite solid lubricating films were deposited by medium frequency unbalanced magnetron sputtering with mixed Ar/CH₄ gases of different volume ratios as the source gases. The effects of Ar/CH₄ ratios on the microstructure, mechanical, and tribological properties of the films were investigated. It has been found that Ar/CH₄ ratios have great effects on the microstructure of the films, including content and stoichiometry ratio of Mo and S, sp² C content, the formation of MoS₂ nanocrystallites, as well as dominate mechanical and tribological properties of the films. The MoS₂/a-C:H film deposited at Ar/CH₄ ratio = 105/5 maintained the highest hardness and generated a unique nanocomposite structure, where MoS₂ nanoparticles were embedded in the cross-linked

amorphous carbon matrix. The nanocomposite structure of the film bestows excellent antiwear ability in test environments (air and vacuum), which shows promising potential as a kind of space lubricants.

Acknowledgments The authors are grateful to the National Natural Science Foundation of China (Grant No. 51275509 and 51175491), the 973 Project of China (No. 2013CB632300), and the Chinese Academy of Science for financial support.

References

- Voevodin, A.A., Zabinski, J.S.: Nanocomposite and nanostructured tribological materials for space applications. *Compos. Sci. Technol.* **65**, 741–748 (2005)
- Voevodin, A.A., Phelps, A.W., Zabinski, J.S., Donley, M.S.: Friction induced phase transformation of pulsed laser deposited diamond-like carbon. *Diam. Relat. Mater.* **5**, 1264–1269 (1996)
- Miyoshi, K., Wu, R.L.C., Garscadden, A.: Friction and wear of diamond and diamond-like carbon coatings. *Surf. Coat. Technol.* **54–55**(2), 428–434 (1992)
- Donnet, C.: Advanced solid lubricant coatings for high vacuum environments. *Surf. Coat. Technol.* **80**, 151–156 (1996)
- Fontaine, J.: Towards the use of diamond-like carbon solid lubricant coatings in vacuum and space environments. *Proc. Inst. Mech. Eng. Part J J. Eng. Tribol.* **222**, 1015–1029 (2008)
- Liu, Y., Gubisch, M., Haensel, T., Spiess, L., Schaefer, J.: Evaluation of the friction of WC/DLC solid lubricating films in vacuum. *Tribol. Int.* **39**, 1584–1590 (2006)
- Voevodin, A.A., Bultman, J., Zabinski, J.S.: Investigation into three-dimensional laser processing of tribological coatings. *Surf. Coat. Technol.* **107**, 12–19 (1998)
- Liu, Y., Gubisch, M., Haensel, T., Spiess, L., Schaefer, J.: Evaluation of the friction of WC/DLC solid lubricating films in vacuum. *Tribol. Int.* **39**, 1584–1590 (2006)
- Takeo, T., Abe, S., Adachi, K., Miki, H., Takagi, T.: Deposition and structural analyses of molybdenum-disulfide (MoS₂)-amorphous hydrogenated carbon (a-C:H) composite coatings. *Diam. Relat. Mater.* **19**, 548–552 (2010)
- Lince, J., Kim, H., Bertrand, P., Eryilmaz, O., Erdemir, A.: Tribochemistry and wear life improvement in liquid-lubricated H-DLC-coated bearings. *Aerosp. Rep.* **8665**, 32 (2007)
- Wang, Y., Li, H., Ji, L., Liu, X., Wu, Y., Lv, Y., Fu, Y., Zhou, H., Chen, J.: Synthesis and characterization of titanium-containing graphite-like carbon films with low internal stress and superior tribological properties. *J. Phys. D Appl. Phys.* **45**, 295301 (2012)
- Hopf, C., Jacob, W., von Keudell, A.: Ion-induced surface activation, chemical sputtering, and hydrogen release during plasma-assisted hydrocarbon film growth. *J. Appl. Phys.* **97**, 094904 (2005)
- Zhao, F., Li, H.X., Ji, L., Mo, Y.F., Quan, W.L., Zhou, H.D., Chen, J.M.: Structural, mechanical and tribological characterizations of a-C:H: Si films prepared by a hybrid PECVD and sputtering technique. *J. Phys. D Appl. Phys.* **42**, 165407 (2009)
- Liu, X., Wang, L., Xue, Q.: A novel carbon-based solid-liquid duplex lubricating coating with super-high tribological performance for space applications. *Surf. Coat. Technol.* **205**, 2738–2746 (2011)
- Peng, X.L., Barber, Z.H., Clyne, T.W.: Surface roughness of diamond-like carbon films prepared using various techniques. *Surf. Coat. Technol.* **138**, 23–32 (2001)
- Pimentel, J.V., Polcar, T., Cavaleiro, A.: Structural, mechanical and tribological properties of Mo–S–C solid lubricant coating. *Surf. Coat. Technol.* **205**, 3274–3279 (2011)
- Eda, G., Yamaguchi, H., Voiry, D., Fujita, T., Chen, M., Chhowalla, M.: Photoluminescence from chemically exfoliated MoS₂. *Nano Lett.* **11**, 5111–5116 (2011)
- Fanchini, G., Tagliaferro, A., Popescu, B., Davis, E.A.: Paramagnetic properties and hydrogen-related structural relaxation effects in magnetron-sputtered a-C:H thin films. *J. Non-Cryst. Solid* **299–302**(2), 846–851 (2002)
- Koós, M., Veres, M., Füle, M., Pócsik, I.: Ultraviolet photoluminescence and its relation to atomic bonding properties of hydrogenated amorphous carbon. *Diam. Relat. Mater.* **11**, 53–58 (2002)
- Irmer, G., Dorner-Reisel, A.: Micro-Raman studies on DLC coatings. *Adv. Eng. Mater.* **7**, 694–705 (2005)
- Ferrari, A.C., Meyer, J.C., Scardaci, V., Casiraghi, C., Lazzeri, M., Mauri, F., Piscanec, S., Jiang, D., Novoselov, K.S., Roth, S., Geim, A.K.: Raman spectrum of graphene and graphene layers. *Phys. Rev. Lett.* **97**, 187401 (2006)
- Ha, P.C.T., McKenzie, D.R., Bilek, M.M.M., Kwok, S.C.H., Chu, P.K., Tay, B.K.: Raman spectroscopy study of DLC films prepared by RF plasma and filtered cathodic arc. *Surf. Coat. Technol.* **201**, 6734–6736 (2007)
- Foong, Y.M., Koh, A.T.T., Lim, S.R., Chua, D.H.C., Ng, H.Y.: Properties of laser fabricated nanostructured Cu/diamond-like carbon composite. *J. Mater. Res.* **26**, 2761–2771 (2011)
- Foong, Y.M., Hsieh, J., Li, X., Chua, D.H.C.: The study on the effect of erbium on diamond-like carbon deposited by pulsed laser deposition technique. *J. Appl. Phys.* **106**, 064904–064908 (2009)
- Veres, M., Toth, S., Koos, M.: Grain boundary fine structure of ultrananocrystalline diamond thin films measured by Raman scattering. *Appl. Phys. Lett.* **91**, 031913 (2007)
- Lifshitz, Y., Edrei, R., Hoffman, A., Grossman, E., Lempert, G.D., Berthold, J., Schultrich, B., Jäger, H.U.: Surface roughness evolution and growth mechanism of carbon films from hyperthermal species. *Diam. Relat. Mater.* **16**, 1771–1776 (2007)
- Wang, P., Wang, X., Xu, T., Liu, W., Zhang, J.: Comparing internal stress in diamond-like carbon films with different structure. *Thin Solid Films* **515**, 6899–6903 (2007)
- Wang, X., Xing, Y., Ma, S., Zhang, X., Xu, K., Teer, D.: Microstructure and mechanical properties of MoS₂/titanium composite coatings with different titanium content. *Surf. Coat. Technol.* **201**, 5290–5293 (2007)
- Neuville, S., Matthews, A.: A perspective on the optimisation of hard carbon and related coatings for engineering applications. *Thin Solid Films* **515**, 6619–6653 (2007)
- Zhang, S., Sun, D., Fu, Y., Du, H.: Toughness measurement of thin films: a critical review. *Surf. Coat. Technol.* **198**, 74–84 (2005)
- Voevodin, A.A., Zabinski, J.S.: Load-adaptive crystalline–amorphous nanocomposites. *J. Mater. Sci.* **33**, 319–327 (1998)